

Stability criterion for the magnetic separation of rare-earth ions

Zhe Lei ^{1,2,*}, Barbara Fritzsche,² and Kerstin Eckert ^{1,2,†}

¹*Institute of Fluid Dynamics, Helmholtz-Zentrum Dresden-Rossendorf (HZDR), Bautzner Landstrasse 400, D-01328 Dresden, Germany*

²*Institute of Processing Engineering and Environmental Technology, Technische Universität Dresden, D-01069 Dresden, Germany*



(Received 12 April 2019; published 17 January 2020)

The stability criterion for the magnetic separation of rare-earth ions is studied, taking dysprosium Dy(III) ions as an example. Emphasis is placed on quantifying the factors that limit the desired high enrichment. During magnetic separation, a layer enriched in Dy(III) ions is generated via the surface evaporation of an aqueous solution which is levitated by the Kelvin force. Later, mass transport triggers instability in the enriched layer. The onset time and position of the instability is studied using an interferometer. The onset time signals that an advective process which significantly accelerates the stratification of enrichment is taking place, although the initial phase is quasi-diffusion-like. The onset position of the flow agrees well with that predicted with a generalized Rayleigh number ($Ra^* = 0$) criterion which includes the Kelvin force term acting antiparallel to gravity. Further three-dimensional analysis of the potential energy, combining magnetic and gravitational terms, shows an energy barrier that has to be overcome to initiate instability. The position of the energy barrier coincides well with the onset position of the instability.

DOI: [10.1103/PhysRevE.101.013109](https://doi.org/10.1103/PhysRevE.101.013109)

I. INTRODUCTION

One important aspect of magnetism is its ability to levitate objects such as a water droplet or graphene [1]. Even heavier objects such as frogs can be levitated if the stray field is provided by a superconducting magnet (16 T) [2]. The body force responsible for these remarkable effects originates from the nonhomogeneous magnetization of diamagnetic substances in a spatial magnetic field gradient and is written as

$$\vec{f}_m = \frac{\chi}{\mu_0} (\vec{B} \cdot \vec{\nabla}) \vec{B} = \frac{\chi}{2\mu_0} \vec{\nabla} \vec{B}^2, \quad (1)$$

provided that the demagnetization field and Lorentz force in the medium are negligible. In Eq. (1), \vec{f}_m refers to the Kelvin force density, χ is the magnetic susceptibility of the material, μ_0 is the magnetic permeability of free space, and \vec{B} is the magnetic flux density. This so-called magnetic field gradient force, or Kelvin force, is the product of a magnetic-field-dependent term and the magnetic susceptibility of the material. Equation (1), which is used very often in the literature dealing with paramagnetic liquids and/or particles, e.g., Refs. [3,4], is equivalent to the classical Rosensweig formulation [5] as shown in the Supplemental Material [6].

The Kelvin force has long been used to separate particles based on their different magnetic properties. Conventional forms of magnetic separation, such as the dry drum separator [7], rely on a permanent magnet with a remanence in the order of 1 T. This technology is generally limited to separating particles with high magnetic susceptibility, such as iron and magnetite. Inserting a ferromagnetic material in the form of a porous matrix into a magnetic field, as done in the high

gradient magnetic separator (HGMS) [8,9], significantly increases the Kelvin force. This is the consequence of a local concentration of the magnetic flux density in the immediate vicinity of the matrix elements. Cycling a carrier liquid with suspended particles through this magnetized region enables micron-sized ferromagnetic particles or paramagnetic particles of a sufficiently larger size to be separated from nonmagnetic ones.

Essentially, as a carrier fluid, water gives rise to a more pronounced buoyancy than air acting antiparallel to gravity. This allows a more feasible manipulation of magnetic particles when the Kelvin force is more significant than the counteracting hydrodynamic forces. The dynamics of magnetic particles driven by the Kelvin force are discussed in the context of magnetophoresis [4,10–13]. Further extension down to the microfluidics scale [14] demonstrates the Kelvin force's applicability in biological contexts. Moreover, a quantitative understanding of magnetophoresis can be used to measure the density [15] of diamagnetic particles in a paramagnetic solution or to measure the susceptibility [16] of paramagnetic solutions in an immiscible organic carrier liquid phase.

Since the late 2000s, a surprising effect of the Kelvin force has been reported, consisting of the formation of a localized enrichment of paramagnetic ions in the magnetic field gradient [17–23]. This phenomenon has inspired the technique of magnetically separating rare-earth (RE) ions, since it extends early works [24] to include even smaller elements, e.g., ions. Indeed, many nonrecyclable chemicals applied in conventional solvent extraction [25,26] could be partially replaced by a magnetic separation step.

Conceptually, the selective magnetic separation of different RE ions from a solution seems feasible based on the difference in magnetic susceptibility by three orders of magnitude [27]. Nevertheless, further development was hindered by an insufficient understanding of the working mechanisms. In

*z.lei@hzdr.de

†k.eckert@hzdr.de

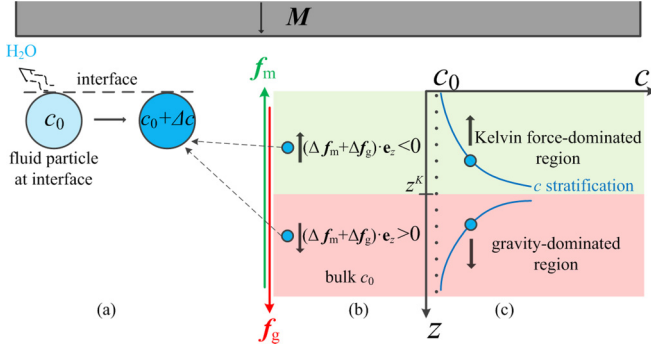


FIG. 1. Sketch of the magnetic separation principle. (a) Evaporation-assisted enrichment formation. (b) The enriched fluid particle, shown as a blue sphere in the homogeneous bulk fluid, is exposed to an increased specific weight \vec{f}_g and an increased Kelvin force \vec{f}_m . (c) Illustration of the $Ra^* = 0$ criterion for the 1D stability analysis for a fluid particle in a monotonically stratified concentration profile in both the Kelvin force and the gravity-dominated regions, respectively.

particular, it was unclear how the small magnetic energy $E_m = \mu_0 M H V$, where M is the magnetization, H is the magnetic field and V is the characteristic volume, provided by the stray field of a permanent magnet, could compete with the much higher kinetic energy of Brownian motion which scales like kT (where k is the Boltzmann constant T is the temperature). Since the concentration field $c(z)$ obeys the Boltzmann distribution, which can be expressed in simplified manner as $c(z) \propto c_0 \exp(-E_m/kT)$, no change is expected from the initially spatially homogeneous distribution c_0 due to $E_m \ll kT$.

A recent work [21] has clarified that an external source, e.g., evaporation, is required to assist the process of enrichment. The evaporation of water at the interface, while solute remains conserved, forces a local increase, Δc , in the concentration of the RE ion, see Fig. 1(a). This enriched fluid layer is of greater density. A system with a denser fluid above a lighter one is hydrodynamically unstable and is prone to Rayleigh-Taylor (RT) instability, leading to convective mixing. However, the Kelvin force, acting antiparallel to gravity, magnetically levitates the enriched layer similarly to the manner in which a paramagnetic liquid is levitated with a magnetized iron wire [3,28] in water.

However, a design guide for a prototype device making use of this principle requires a quantitative understanding of the limit of magnetic separation. This naturally led to the question of whether a stability criterion can be formulated predicting this limit. To analyze the stability of the system, the Rayleigh number concept was borrowed [21] from the context of linear stability theory, as used to describe the Rayleigh-Bénard convection [29]. In the presence of a vertical density stratification, caused by a concentration difference Δc over a length l_c , the Rayleigh number, Ra_c , is a nondimensional measure of the forcing $\vec{f}_g = \rho_0 g (1 + \alpha \Delta c) \cdot \vec{e}_z$, given by

$$Ra_c = -\frac{l_c^4}{D\mu} \frac{\partial(\vec{f}_g \cdot \vec{e}_z)}{\partial z}, \quad (2)$$

where D , μ , ρ , α , and \vec{e}_z refer to the mass diffusivity, dynamic viscosity, density, densification factor, and the unit vector parallel to gravity, respectively. Ra_c can be understood as the ratio between the characteristic time scale of the dissipative effects, mass diffusion, and viscosity and that of the buoyant forcing. Typically, if the resulting Rayleigh number exceeds the critical one, $O(Ra_c) \sim 10^3$, then the base state, characterized by entirely diffusive but no convective transport, becomes unstable according to linear stability theory, and convection sets in. Note that we have adapted the sign in Eq. (2) since $\partial(\vec{f}_g \cdot \vec{e}_z)/\partial z < 0$ in the present evaporation-driven case, and thus $Ra_c > 0$ as expected. When the Kelvin force is added, the situation becomes more complex than the classical Rayleigh-type instabilities: First, a destabilizing gravitational force competes with a counteracting Kelvin force \vec{f}_m which stabilizes the system. Second, in contrast to \vec{f}_g , the Kelvin force is three dimensional (3D). The Kelvin force \vec{f}_m could also be expressed via a magnetic Rayleigh number if only the z component antiparallel to gravity is considered, i.e.,

$$Ra_m = -\frac{l_c^4}{D\mu} \frac{\partial \vec{f}_m \cdot \vec{e}_z}{\partial z}. \quad (3)$$

Third, the 3D base state is time dependent and governed not only by mass diffusion but also by convection, as will be demonstrated later. Thus, any stability analysis is extremely challenging since even established concepts for diffusive base states such as the frozen-time approach, see, e.g., Ref. [30], cannot be applied. Currently, it is impossible to quantify the desired critical Rayleigh number as a function of Ra_m as can be done for thermomagnetic convection, see, e.g., Ref. [31]. Only the trend can be anticipated, namely an increase in Ra_c as Ra_m increases.

In order to approximately capture the critical stability condition and to estimate the maximum concentration stratification achievable, a simplified stability criterion, based on a generalized Rayleigh number Ra^* , was introduced in Ref. [21]. By including the antiparallel component of the counteracting Kelvin force \vec{f}_m , $Ra^* = Ra_m + Ra_c$ considers the total forcing:

$$Ra^* = -\frac{l_c^4}{D\mu} \frac{\partial(\vec{f}_g + \vec{f}_m) \cdot \vec{e}_z}{\partial z}, \quad (4)$$

where $\vec{f}_g = \rho(z)g \cdot \vec{e}_z$ is the specific weight which is modified by Δc [cf. Figs. 1(a) and 1(b)]. We assume that the system remains stable as long as the counteracting Kelvin force compensates for the specific weight of the enriched layer and takes the criterion $Ra^* = 0$ as a threshold to access the critical concentration stratification which can still be levitated.

On inspecting Eq. (4), one notes that this stability criterion is equivalent to seeking the local extrema of the resulting total force, see Fig. 1(c). Since both \vec{f}_g and \vec{f}_m are functions of the local enrichment $\Delta c(z)$, the partial derivative of the forces, $\vec{f}_g = \rho_0 g (1 + \alpha \Delta c) \cdot \vec{e}_z$ and $\vec{f}_m = \frac{\chi}{2\mu_0} \vec{\nabla} \vec{B}^2 = \frac{\chi_0 + \chi_{Dy} \Delta c}{2\mu_0} \vec{\nabla} \vec{B}^2$, with respect to z leads to a critical concentration gradient at $Ra^* = 0$:

$$\left. \frac{\partial \Delta c}{\partial z} \right|_{Ra^*=0} = -\chi \frac{\frac{\partial f_{z0}}{\partial z}}{\rho_0 g \alpha + \chi_{Dy} f_{z0}}, \quad (5)$$

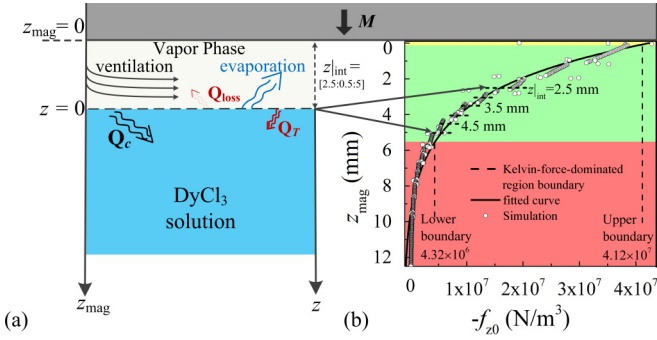


FIG. 2. (a) Schematic of the experimental setup together with the physical processes and the coordinate system. The distance between the lower edge of the magnet and the solution interface is denoted as z_{int} . Q_c and Q_T are mass and heat fluxes at the interface forced by evaporation, and Q_{loss} is the heat loss. (b) The $-f_{z0}$ term of the Kelvin force versus z_{mag} originating from the center of the magnet's lower edge. The fitted curve (solid line) is given by $f_{z0} = 4.357 \exp(0.3715z - 0.1223)$.

where χ_0 is the magnetic susceptibility of the fluid at its initial concentration and

$$\vec{f}_{z0} = f_{z0} \cdot \vec{e}_z = \frac{1}{2\mu_0} \frac{\partial \vec{B}^2}{\partial z} \cdot \vec{e}_z. \quad (6)$$

Note that $f_{z0} < 0$ due to the decay of \vec{B} with increasing z in a magnetic dipole field as used in the work. It is apparent that a singularity, i.e., a pole, exists when the denominator vanishes. The position, z^K , of this singularity depends both on the material data, density ρ_0 , densification factor α , and magnetic susceptibility of the paramagnetic solution (here DyCl_3 , χ_{Dy}) and on f_{z0} and its derivative. The concrete value of z^K , see Eq. (5), is implicitly given by

$$|f_{z0}^K(z^K)| = \frac{\rho_0 g \alpha}{\chi_{\text{Dy}}}. \quad (7)$$

Since both the right-hand side of Eq. (7) and f_{z0} of the magnet are known, z^K can be determined, cf. Fig. 2. z^K separates the space taken by the paramagnetic solution inside the cuvette into two regions: The Kelvin force-dominated region, bounded by $z \leq z^K$, is defined by the condition $|f_{z0}| \geq |f_{z0}^K(z^K)|$. Given a local enrichment Δc , the resulting Kelvin force change in this region is greater than the increase in the specific weight, see Fig. 1(b). The enriched fluid particle experiences a forcing antiparallel to gravity which is able to magnetically levitate the enriched fluid layer above the dilute bulk as observed in Refs. [18,19,21]. Note that Eqs. (5) and (7) imply a $\frac{\partial c}{\partial z} > 0$, as shown schematically in Fig. 1(c), to fulfill the condition $\text{Ra}^* = 0$ in the presence of a dominating Kelvin force.

By contrast, the zone in which the change in the Kelvin force is smaller than that of specific weight refers to the gravity-dominated region. This is characterized by $|f_{z0}| \leq \frac{\rho_0 g \alpha}{\chi_{\text{Dy}}}$ or by $z \geq z^K$. The concentration gradient needed to satisfy $\text{Ra}^* = 0$ turns its sign to $\frac{\partial c}{\partial z} < 0$, see Fig. 1(c). Hence, the more concentrated fluid particle settles parallel to gravity when the critical condition is reached. This corresponds to $\frac{\partial(f_g + \vec{f}_m) \cdot \vec{e}_z}{\partial z} \leq 0$, i.e., $\text{Ra}^* \geq 0$, in the lower region of Fig. 1(c).

To further understand the stability criterion, experimental evidence needs to be provided of the Kelvin force-dominated region. Moreover, the correlation of the Kelvin force-dominated region with a desired high level of enrichment needs to be investigated. To this end, an enhanced evaporation rate compared to that in the Ref. [21] is imposed to force the instability of the enrichment layer. The position and onset time of this instability are studied for different Kelvin force strengths using an interferometer. The experimental results are compared with both the $\text{Ra}^* = 0$ criterion and an analysis of the potential energy of the system. We show that the spatial zone where the experimentally observed instability occurs correlates very well both with the predicted location of an energy barrier and with the $\text{Ra}^* = 0$ criterion.

II. EXPERIMENTAL SYSTEM AND STABILITY ESTIMATION

The experiments use a quartz cell with inner dimensions of $10 \times 10 \times 10 \text{ mm}^3$. The cell is filled with a 0.5 M DyCl_3 solution, the pH value of which is adjusted to 1 using HCl to prevent the formation of intermediates, such as dysprosium hydroxide [21]. A permanent magnet measuring $10 \times 10 \times 10 \text{ mm}^3$ (Webercraft GmbH, remanence $B_r = 1280 \text{ mT}$, magnetization N42) provides a static inhomogeneous magnetic field. The z axis of the magnet's coordinate system, termed z_{mag} , starts at the lower edge of the magnet. It is parallel to the direction both of the magnetization and the gravity, see Fig. 2(a). The z component of the Kelvin force $f_{z0} = \frac{\vec{f}_m \cdot \vec{e}_z}{\chi} = \frac{1}{2\mu_0} \frac{\partial \vec{B}^2}{\partial z}$, see Eq. (6), can be quantified using the knowledge about the spatial distribution of the magnetic induction \vec{B} of the magnet and its material data. Figure 2(b) presents the axial component of f_{z0} . A negative value of f_{z0} implies that the z component of the Kelvin force density is directed upward antiparallel to gravity, in agreement with the introduction in Sec. I, Fig. 1. It reaches its maximum level at the magnet's surface and decays rapidly with increasing distance from the magnet.

Analyzing the forces with the criterion $\text{Ra}^* = 0$, we are able to quantify the different regions, shown in Fig. 1, which exist as a result of the competing Kelvin force and specific weight. The border between both regions is set by z^K , defined in Eq. (7). The green region marked in Fig. 2(b), the Kelvin force-dominated region, is characterized by a more significant change in the Kelvin force \vec{f}_m in comparison to that of the specific weight \vec{f}_g due to a local concentration change. The specific weight $\vec{f}_g = \rho g \cdot \vec{e}_z$ represents the force exerted by gravity on a unit volume of a fluid. The Kelvin force-dominated region is bounded from above at $z_{\text{mag}} \approx 0.1 \text{ mm}$ by the condition $|\vec{f}_m| = |\vec{f}_g|$. At even shorter distances to the magnet, corresponding to the thin region colored in yellow, the surface of the paramagnetic DyCl_3 solution jumps toward the magnet. Bounding from below occurs at $z_{\text{mag}} = z^K \approx 5.5 \text{ mm}$ by a region marked in red. In this region, enrichment leads to an increase in the specific weight as a result of the enrichment no longer being compensated for by the weaker Kelvin force. Hence, a $\Delta c > 0$, which is equivalent to an unstable stratification, leads to a downward flow in the

TABLE I. Variables as a function of temperature and concentration. Nonsignificant terms are marked with *.

Dependent variable	Variable (X)	
	*T	c
Refractive index n ($\Delta n = \frac{\partial n}{\partial X} \Delta X$)	$\frac{\partial n}{\partial T} = -\frac{1}{10200} \text{ K}^{-1}$	$\frac{\partial n}{\partial c} = \frac{1}{23.31002} \text{ M}^{-1}$
Diffusivity κ	$\kappa_T = 1.38 \times 10^{-7} \text{ m}^2/\text{s}$	* $\kappa_c = 1 \times 10^{-9} \text{ m}^2/\text{s}$
Density/volume expansion α_X ($\Delta \rho = \rho_0 \alpha_X \Delta X$)	$\alpha_T = -2.56 \times 10^{-4} \text{ K}^{-1}$ [27]	$\alpha = 2.43 \times 10^{-1} \text{ M}^{-1}$
Magnetic susceptibility χ_X ($\Delta \chi = \chi_X \Delta X$)	* $\chi_T \approx -2.3 \times 10^{-5} \text{ K}^{-1}$	$\chi_{\text{Dy}} = 5.5 \times 10^{-4} \text{ M}^{-1}$
Kelvin force-dominated lower boundary ($f_{z0} X$)	* $f_{z0} T = 1.09 \times 10^5 \text{ N/m}^3$	$f_{z0} c = 4.32 \times 10^6 \text{ N/m}^3$

solution. Therefore, the red-marked region is referred to as the gravity-dominated region.

The transport processes in the DyCl_3 enrichment zone, which is exposed to evaporation, are probed for varying Kelvin forces. These are adjusted by changing the distance between the magnet and the position of the interface of the solution, referred to as z_{int} in the coordinate system of the magnet, see Fig. 2(a). To enhance the evaporation rate at the open interface in comparison to Ref. [21], an air flow is imposed parallel to the solution surface with a Reynolds number of around 300 at a time interval $t \in [10, 120]$ s. Due to the controlled ambient temperature and humidity, the evaporation rate is kept constant for all experiments.

A Mach-Zehnder interferometer (MZI) is used to measure the time- and space-resolved refractive index field of the solution [21,32,33]; this is a function of both the temperature T and the concentration c . Evaporation of water molecules at the surface requires the latent heat to be provided. As a result, the local temperature below the interface decreases, marked in Fig. 2(a) as Q_T . This thermal effect introduces an unwanted ΔT , correlating with the refractive index. To decouple and quantify the two variables separately from the interferometer measurements, we use the method developed in Ref. [21]. After the ventilation stops at $t = 120$ s, the measured refractive index field remains nearly unchanged, see Fig. 4(b). This indicates that the dominant source term of the refractive index field has a low diffusivity, corresponding to mass transfer, see Table I. This implies that the thermal effect has dissipated in the same time interval and becomes negligible. Hence, the temperature of the solution is considered to be constant. Therefore, the safe conversion of the measured refractive index change to the concentration field is guaranteed, as proved in Ref. [21]. Admittedly, a transient temperature effect might play a role at the beginning. The resulting effect on the relevant parameters, α and χ , is summed up in Table I. The Curie-Weiss law defines the magnetic susceptibility of Dy via $\chi = \frac{C}{T - T_C}$, where the C is Curie constant with a value in the order of 1 K [34]. Therefore, $\chi_T = \frac{\partial \chi}{\partial T} |_{T=298.15} \approx -2.3 \times 10^{-5} \text{ K}^{-1}$. To account for the same order of magnitude of influence on χ , the temperature change in K has to be four orders of magnitude greater than the concentration change in mM. Hence, temperature dependence on the magnetic susceptibility can be neglected. The position of the pole produces a lower boundary value $f_{z0}|T = 1.09 \times 10^5 \text{ N/m}^3$ for the thermal Kelvin force-dominated region when the thermal expansion coefficients α_T and χ_T replace α and χ_{Dy} in Eq. (7). Hence, a density increase caused by a minor residual cooling effect is overcompensated by the

increase in the χ_T -based Kelvin force, see Eq. (1). Therefore, the thermal expansion coefficient becomes nonsignificant and the T effect is decoupled from the concentration field measurement with the interferometer.

III. RESULTS

The experiments start when the position of the magnet relative to the solution interface is fixed. Ten seconds later, ventilation is switched on to enhance evaporation until $t = 120$ s. In the next period, within $t \in [120, 240]$ s, ventilation is switched off; finally, the magnet is removed at 240 s. The 2D concentration distribution, measured with the MZI, is plotted in Fig. 3(a) at 240 s for the case $z_{\text{int}} = 2.5$ mm. Similarly

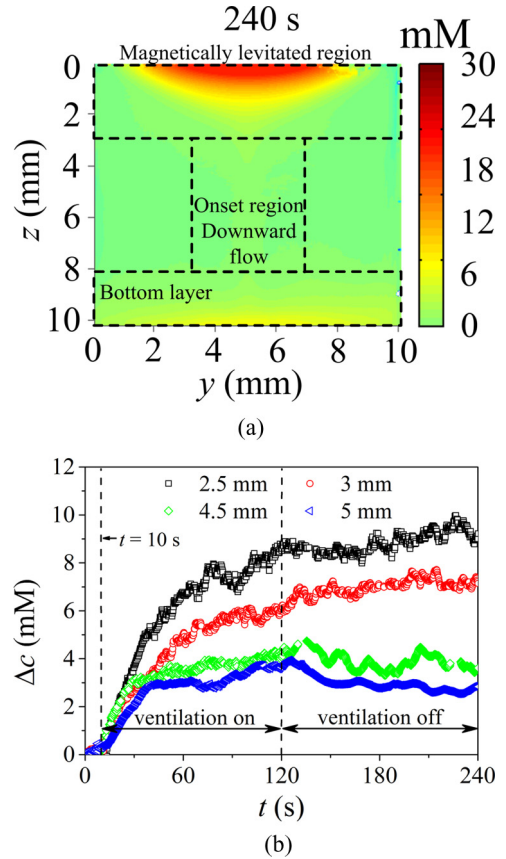


FIG. 3. (a) Concentration distribution in the cell at $t = 240$ s. The distance from the interface to the magnet on top is $z_{\text{int}} = 2.5$ mm, cf. Fig. 2(a). (b) Average enrichment in the region $z \in [0, 2]$ mm versus time for different magnet-to-interface distances z_{int} .

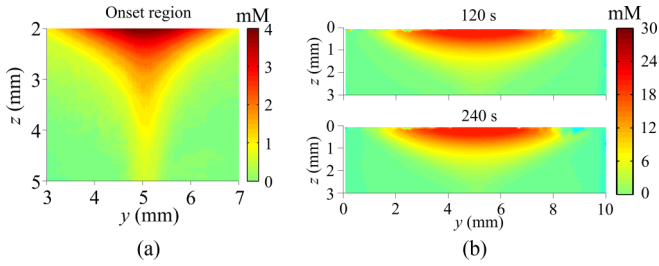


FIG. 4. (a) Zoom into the *onset region* of the downward flow, marked in Fig. 3(a) for the case $z_{\text{int}} = 2.5$ mm at 240 s. (b) Corresponding concentration distribution in the *magnetically levitated region*, marked in Fig. 3(a), at 120 s and 240 s.

to previous works, an oval enrichment zone of Dy(III) ions is generated in the upper region closer to the interfaces.

The average enrichment, Δc , in this zone, $z \in [0, 2]$ mm, is plotted versus time in Fig. 3(b). This shows that enrichment proceeds rapidly between $t \in [10, 120]$ s and remains nearly unchanged between $t \in [120, 240]$ s. A 4 \times -higher enrichment is found in comparison to that in Ref. [21]. This enrichment in the immediate vicinity of the interface amounts to $\Delta c \approx 30$ mM [see Fig. 3(a)], corresponding to $\approx 6\%$ of the bulk concentration, or to 9 mM after averaging over $z \in [0, 2]$ mm. If the distance between the magnet and the interface of the solution is increased in steps from $z_{\text{int}} = 2.5$ mm toward $z_{\text{int}} = 5$ mm, then the average enrichment Δc decreases from 9 mM to approximately 3 mM. This drop is notable because the evaporation rate is the same in these experiments. However, at a greater distance from the magnet, the Kelvin force is obviously no longer able to levitate the full amount of the evaporation-assisted enrichment.

The reason for that lies in an instability of the enrichment zone. This can be seen in Fig. 4(a), which zooms into the region $z \in [2, 5]$ mm along $y \in [3, 7]$ mm, marked by the middle dashed rectangle in Fig. 3(a). After a critical time, determined below, a downward flow from the levitated enriched zone sets in. This flow bears similarities to a buoyant plume emitted from a hydrodynamically unstable boundary layer, see Fig. 5. However, even after the onset of instability, the concentration in the magnetically levitated region inside the Kelvin force-dominated region is changed only marginally in a time span $t \in [120, 240]$ s, see Fig. 4(b). This means that

an enrichment of up to O(30 mM) within this region is stably levitated.

The critical time and position of the onset of the downward flow out of the enrichment layer are detected based on the concentration distribution plotted in Fig. 5. From 24 to 60 s, a gradual increase in the curvature of the isoconcentration contour is observed within $z \in [3, 4]$ mm, which corresponds to the onset position range. This is a consequence of the slow formation of a convective pattern in the gravity-dominated region at the border to the Kelvin force-dominated region. The enrichment is then advected parallel to gravity and settles at the bottom of the cell. The onset of flow evolves slowly, partly since the resulting force, $\Delta f_m + \Delta f_g$, nullifies near $z = 3$ mm (for the case $z_{\text{int}} = 2.5$ mm), i.e., at the lower boundary of the Kelvin force-dominated region. In view of the blurred isoconcentration contour at the critical condition, forced by the sharp curvature, an onset time *span* is extracted instead. Within $t \in [30, 38]$ s, the downward flow formation process is clearly visible in Fig. 5. The onset time is calculated as the average, i.e., 34 s in the present case [cf. Fig. 6(a)]. The error bar characterizes the width of the onset time span.

Using this approach, both the time and the vertical position of the onset of instability are plotted in Fig. 6 for varying z_{int} . The z coordinate refers to the coordinate system of the cell filled with the DyCl_3 solution, i.e., $z = 0$ corresponds to the interface of the solution. Note that the error bars of the onset time and position stem from the time span and onset position range obtained with the detection approach above. The open dots correspond to the mean value of the *measured* onset time span and position range. The solid black dots mark the *predicted* lower boundary, z^K , of the Kelvin force-dominated region, calculated for the respective z_{int} . This z^K value is obtained by finding the z position at which the $f_{z_0}^K$ value predicted by Eq. (7) is adopted inside the cell for the given magnet-to-interface distance z_{int} . We recall that if z_{int} is increased, the magnetic field inside the cell becomes weaker, and z^K is expected to move toward the interface. This trend is reflected by Fig. 6. To give an example, for the case $z_{\text{int}} = 2.5$ mm, a $z^K = 3$ mm (cf. solid dot) is obtained, while for $z_{\text{int}} = 5.0$ mm the boundary is shifted to $z^K = 1$ mm. Furthermore, it turns out that the predicted z^K value is always located in the onset position range as measured by the interferometer. Thus, good agreement is found between

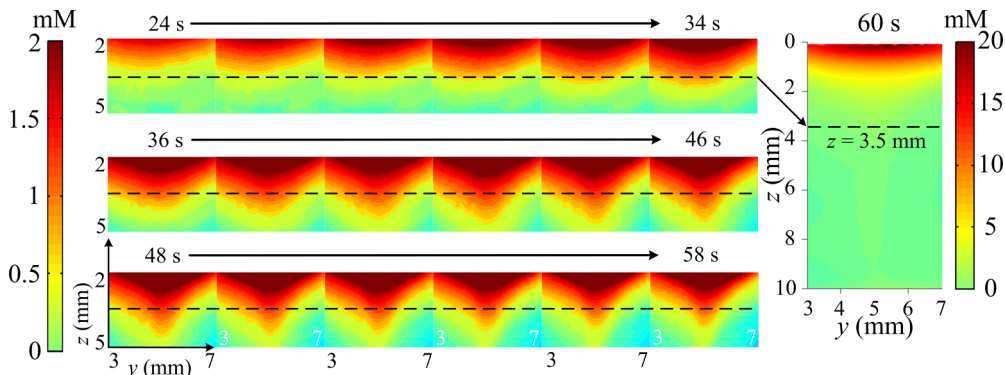


FIG. 5. Zoom into the onset region, indicated in Fig. 3(a), for the case $z_{\text{int}} = 2.5$ mm between $t \in [24, 58]$ s with a stretched Δc color-bar range of [0,2] mM. A larger section, $z \in [0, 10]$ mm and $y \in [3, 7]$ mm, including the zoom is shown on the right.

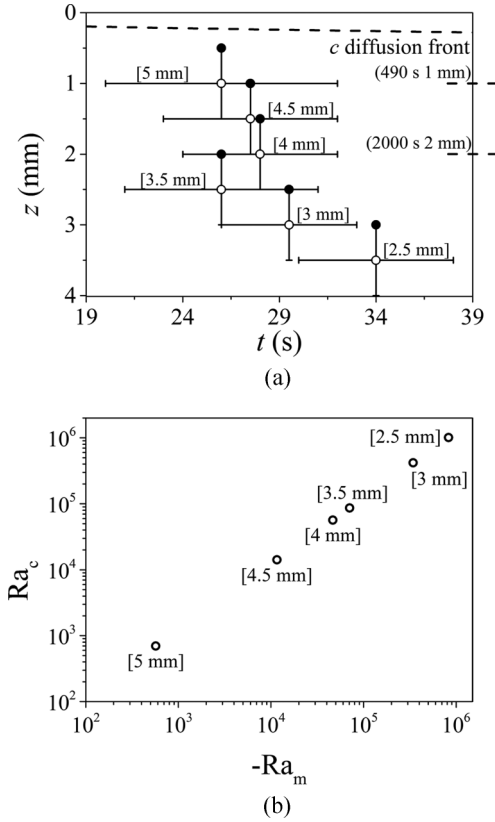


FIG. 6. (a) Time span and vertical position range of the onset of instability in the form of downward flow measured with the interferometer for the different $[z|_{\text{int}}]$ as indicated in the diagram (open dots). Predicted position z^K of the lower boundary of the Kelvin force-dominated region (solid dots) using Eq. (7). The position of the diffusion front of c is marked by a dashed line and in the right-hand margin of the diagram for a longer stratification length. (b) Translation of the instability information of (a) into the nondimensional form, via the Rayleigh numbers Ra_c vs Ra_m .

the measured values and the predicted lower boundary z^K of the Kelvin force-dominated region.

In Fig. 6(b) we translate this information into a nondimensional manner, i.e., critical Rayleigh number Ra_c vs magnetic Rayleigh number Ra_m . To compute both Rayleigh numbers via Eqs. (2) and (3), an average concentration gradient, $\frac{c|_{z=z^K} - c|_{z=0}}{z^K}$, at the center of the cell ($y = 5$ mm) is used together with the characteristic length as the concentration stratification length, i.e., $l_c = z^K$ and material data as given in Table I. We clearly see a strong stabilization effect brought on by the Kelvin force. In Fig. 6(b), this leads to an increase in Ra_c the smaller the magnet-to-interface distance $z|_{\text{int}}$ is. At the smallest distance, $z|_{\text{int}} = 2.5$ mm, adjustable in the experiment, a critical Rayleigh number $O(Ra_c) \sim 10^6$ is found, which is about three orders of magnitude higher than without the magnetic field.

To underline the applicability of the Ra^* in describing the onset of instability and levitation of the enriched layer, we calculate the three Rayleigh numbers Ra_c , Ra_m , and Ra^* locally in Fig. 7. For that purpose, we use the concentration stratification in the center of the solution at $t = 240$ s, which corresponds to Fig. 3. In the Kelvin force-dominated region,

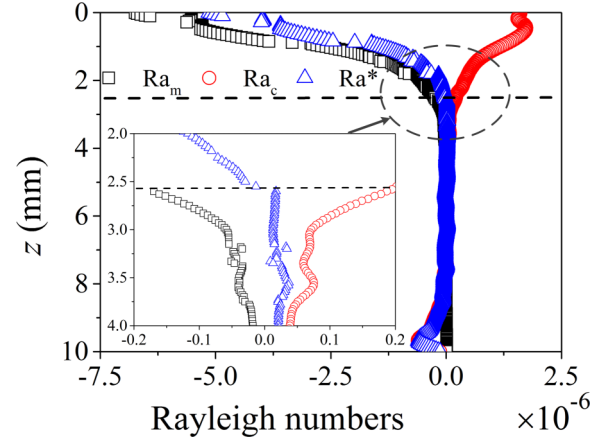


FIG. 7. The behavior of the local Rayleigh numbers Ra_c , Ra_m , and Ra^* as a function of the z coordinate, corresponding to $t = 240$ s in Fig. 3(a). The Rayleigh numbers based on $l_c = z^K$ as the characteristic length and on the vertical concentration gradient in the cell center at $y = 5$ mm. The dashed line is the boundary between the Kelvin force-dominated and the gravity-dominated regions given by z^K , belonging to $z|_{\text{int}} = 2.5$ mm of Fig. 3(a).

the resulting Ra^* , which is the sum of Ra_c and Ra_m , is negative as expected. At the crossover from the Kelvin force-dominated to the gravity-dominated regions, the resulting local Ra^* changes its sign, which occurs at the position $z^K = (2.5 \dots 2.6)$ mm (see inset of Fig. 7) where the instability sets in. This is in excellent agreement with the energy analysis in Sec. IV, Fig. 9(b). Thus, despite the limitations we discussed earlier, the Ra^* criterion demonstrates its validity as a 1D estimation of the limit for magnetic separation.

Next, we come back to Fig. 6(a). Assuming that diffusion is the sole transport process, the concentration isolines of the enrichment layer should propagate according to $\sqrt{2\kappa_c t}$. The position reached by this hypothetical diffusion front is marked by a dashed line in the right-hand margin of Fig. 6(a) for two selected times (490 and 2000 s). At 2000 s the diffusion front has propagated over a distance of 2 mm. At the same position (2 mm), the onset of instability has been detected if $z|_{\text{int}} = 4$ mm (open dot). However, the onset of instability already occurs at (27 ± 5) s, i.e., after well below 2000 s. Obviously, a faster, convective transport process has to be present, which exhibits two prominent features. The first one is the oval shape of the isoconcentration contour, which reaches its maximum extension in the cell along the central symmetry axis of the magnet. The second one is the lack of mixing between the magnetically levitated enriched layer and the bulk.

The latter aspect is illustrated in Fig. 8(a), which displays the differences in the enrichment accumulated at the bottom after the instability has set in, depending on the magnet-to-interface distances $z|_{\text{int}}$. The greater this distance is, e.g., $z|_{\text{int}} = 4.5$ mm compared to that of $z|_{\text{int}} = 2.5$ mm, the larger the amount of enrichment accumulated at the bottom. This is correlated with the fact that for $z|_{\text{int}} = 2.5$ mm the Kelvin force is stronger and can levitate a larger enrichment. Thus, the instability position z^K is deeper in the cell (see left image) compared to $z|_{\text{int}} = 4.5$ mm. At the latter position, the z^K position is shifted further toward the interface ($z^K < 1.5$ mm)

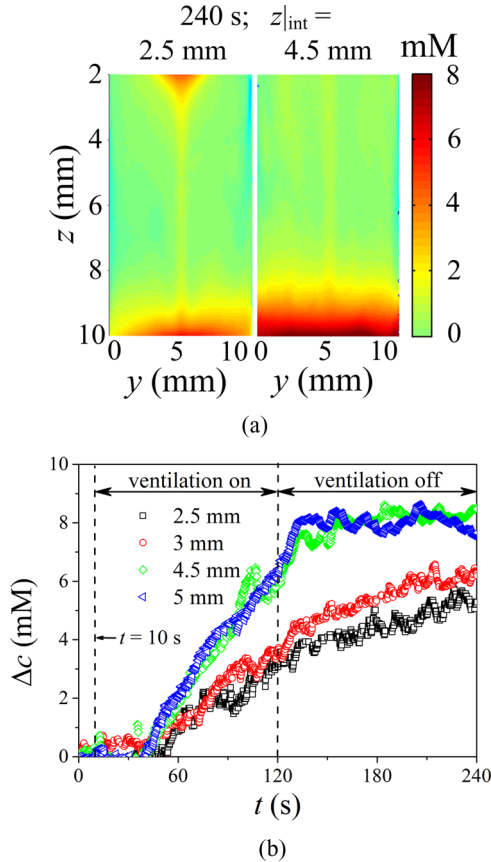


FIG. 8. (a) Concentration distribution at $t = 240$ s for $z|_{\text{int}} = 2.5$ mm and 4 mm in the region $z \in [2, 10]$ mm, covering the gravity-dominated zone. (b) Average enrichment in the region $z \in [9, 10]$ mm versus time for different $z|_{\text{int}}$.

and is therefore no longer visible in the right-hand image of Fig. 8(a).

Figure 8(b) shows the evolution of the mean enrichment, obtained after averaging the concentration in the bottom region $z \in [9, 10]$ mm over the cuvette width, as a function of time for varying $z|_{\text{int}}$. Before the onset of instability, the accumulation is zero. After the onset of instability (Fig. 5), a rapid increase in the average concentration occurs as a result of the advective transport of the enrichment out of the Kelvin force-dominated region downward into the gravity-dominated region. The figure shows a greater amount of enrichment in the gravity-dominated region for greater $z|_{\text{int}}$ due to its impaired ability to levitate the enriched fluid in the Kelvin force-dominated zone.

IV. ENERGY ANALYSIS

To recapitulate, the stability of the present magnetic separation system is governed by the competition between the Kelvin force \vec{f}_m and the specific weight \vec{f}_g . To obtain an approximate prediction for the stability, the $\text{Ra}^* = 0$ criterion was applied. With the help of this criterion, the extension of the Kelvin force-dominated region was determined, enabling the instability onset position to be predicted for different magnitudes of the Kelvin force in Fig. 6. The difference between the observed and predicted values was always less than

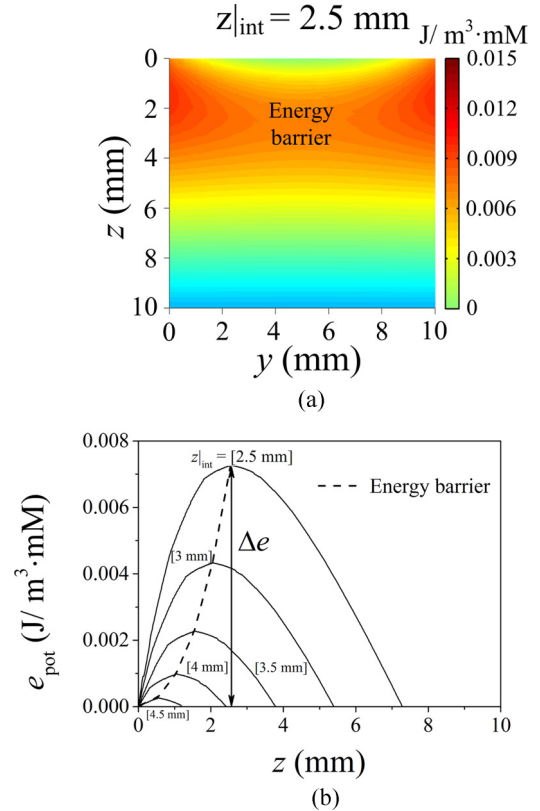


FIG. 9. (a) Molar potential energy density of the overlapped gravity and magnetic fields. (b) Vertical cross section through the energy density in the center of the cell. The dashed line shows the position of the energy barrier for different positions of the interface in the coordinate system of the magnet.

0.5 mm. Hence, the $\text{Ra}^* = 0$ criterion appears as a reasonable first estimation of the instability behavior of the present magnetic separation problem. Nevertheless, the system under study is not one dimensional, as assumed for Ra^* , but three-dimensional. Therefore, we next describe the stability based on a molar potential energy density field e_{pot} .

A homogeneous DyCl_3 solution of concentration c_0 is considered as an equilibrium base state corresponding to the initial condition of the experiment without evaporation. The magnetic and gravity forces acting on the fluid are balanced by the cuvette walls in the base state. Neglecting any temperature effect, a perturbation of the base state is introduced by the concentration enrichment Δc in the fluid. The total force acting on the fluid changes by a $\Delta \vec{f}$ given by $\Delta \vec{f} = \Delta \vec{f}_m + \Delta \vec{f}_g = \left(\frac{\chi_{\text{Dy}}}{2\mu_0} \vec{\nabla} \vec{B}^2 + \rho_0 g \alpha z \right) \Delta c$. The solenoidal multiplier in front of Δc can be rewritten as a molar potential energy density field, e_{pot} , according to $\Delta \vec{f} = -\vec{\nabla} e_{\text{pot}} \Delta c$, where

$$e_{\text{pot}} = - \left(\frac{\chi_{\text{Dy}}}{2\mu_0} \cdot \vec{B}^2 + \rho_0 g \alpha z \right) + \text{const.} \quad (8)$$

The molar potential energy density field, e_{pot} , is plotted in Fig. 9(a) for $z|_{\text{int}} = 2.5$ mm, where the constant in Eq. (8) was adapted such that the reference value is zero at the center of the interface. It is spatially inhomogeneous but steady over time. The important aspect in Fig. 9 is the existence of an energy barrier, i.e., a maximum in e_{pot} which splits

off the region at the interface of the solution from that at the lower part of the cell. For $z|_{\text{int}} = 2.5$ mm this energy barrier Δe is visible at $z = 2.55$ mm in the coordinate system of the cell. Obviously, this value is close to the observation in the experiment [Fig. 6(a)] and in excellent agreement with the $Ra^* = 0$ criterion in Fig. 7. This energy barrier is fixed in the z_{mag} coordinate system. Thus, when $z|_{\text{int}}$ is increased with respect to the plotted value, $z|_{\text{int}} = 2.5$ mm, the energy barrier moves closer to the solution interface, i.e., it moves antiparallel to z direction, see Fig. 9(b). As a result, the size of the region in which the enrichment can be collected shrinks, and the height of the energy barrier Δe is reduced. This implies that the enrichment zone is liable to be more unstable, and that the downflow will thus occur at smaller z values in the enrichment zone. Moreover, the minimum value of the energy barrier is at the center line of the cuvette. Hence, the downward flow prefers to pass through the energy barrier in the middle of the gravity-perpendicular plane.

V. SUMMARY

To sum up, a quantitative understanding of the stability criterion of magnetic separation has been achieved. For this purpose, the evolution of the DyCl_3 enrichment has been analysed for different magnetic fields, which were adjusted by the relative distance between the DyCl_3 solution and the edge of the magnet. With the high evaporation rate imposed, a maximum local Dy(III) ions enrichment of $\Delta c \approx 30$ mM, i.e., $\approx 6\%$ was achieved with the current configuration. The evolution of the enrichment averaged within $z \in [0, 2]$ mm is experimentally resolved and compared with an energy analysis. The key results lie in the discovery of a hydrody-

namic instability of the enrichment zone, in understanding the mechanism of this instability based on analyzing the potential energy field, and in formulating a simplified $Ra^* = 0$ criterion to predict the onset of instability.

The onset of the hydrodynamic instability of the enrichment zone, expressed in a downward flow, has a spatial position consistent to that predicted from both the analysis of the potential energy density field and the $Ra^* = 0$ criterion. The onset of instability occurs significantly before the diffusive concentration front would reach the position of the starting downward flow. This indicates the existence of convection in the Kelvin force-dominated region. However, no active mixing is found between the upper regions of the enrichment with the dilute bulk. Hence, a better understanding of the complex advective transport processes in the different zones of the cell is a precondition for the efficient application of magnetic RE separation. Additional investigations into the dynamics of enrichment could further benefit from this knowledge about the stability criterion. Furthermore, coupling convection with a moving magnetic field allows the enrichment to be manipulated more flexibly in the context of a continuous magnetic separator.

ACKNOWLEDGMENTS

We thank the financial support by the German Space Agency (DLR) with funds provided by the Federal Ministry of Economics and Technology (BMW) due to an enactment of the German Bundestag under Grant No. DLR 50WM1741 (Project SESIMAG-II). We thank Dr. G. Mutschke, Dr. K. Schwarzenberger and Dr. X. Yang for the helpful discussion.

-
- [1] C. Niu, F. Lin, Z. M. Wang, J. Bao, and J. Hu, *J. Appl. Phys.* **123**, 044302 (2018).
 - [2] M. V. Berry and A. K. Geim, *Eur. J. Phys.* **18**, 307 (1997).
 - [3] J. M. D. Coey, R. Aogaki, F. Byrne, and P. Stamenov, *Proc. Natl. Acad. Sci. USA* **106**, 8811 (2009).
 - [4] H. Watarai, M. Suwa, and Y. Iiguni, *Anal. Bioanal. Chem.* **378**, 1693 (2004).
 - [5] R. E. Rosensweig, *Ferrohydrodynamics* (Courier Corporation, Mineola, NY, 2013).
 - [6] See Supplemental Material at <http://link.aps.org/supplemental/10.1103/PhysRevE.101.013109> for derivation of the Kelvin force formulation in a weakly magnetized paramagnetic aqueous solution.
 - [7] J. Oberteuffer, *IEEE Trans. Magn.* **10**, 223 (1974).
 - [8] J. Oberteuffer, *IEEE Trans. Magn.* **9**, 303 (1973).
 - [9] C. Hoffmann, M. Franzreb, and W. Holl, *IEEE Trans. Appl. Supercond.* **12**, 963 (2002).
 - [10] M. Suwa and H. Watarai, *Anal. Chim. Acta* **690**, 137 (2011).
 - [11] M. Fujiwara, K. Mitsuda, and Y. Tanimoto, *J. Phys. Chem. B* **110**, 13965 (2006).
 - [12] J. W. Haverkort, S. Kenjereš, and C. R. Kleijn, *Phys. Rev. E* **80**, 016302 (2009).
 - [13] A. F. Pshenichnikov and A. S. Ivanov, *Phys. Rev. E* **86**, 051401 (2012).
 - [14] N. Pamme, *Lab Chip* **6**, 24 (2006).
 - [15] S. Ge, Y. Wang, N. J. Deshler, D. J. Preston, and G. M. Whitesides, *J. Am. Chem. Soc.* **140**, 7510 (2018).
 - [16] I. R. Rodrigues, L. Lukina, S. Dehaeck, P. Colinet, K. Binnemans, and J. Fransaer, *J. Phys. Chem. C* **122**, 23675 (2018).
 - [17] K. Kołczyk, M. Wojnicki, D. Kutyła, R. Kowalik, P. Żabiński, and A. Cristofolini, *Arch. Metall. Mater.* **61**, 1919 (2016).
 - [18] B. Pulko, X. Yang, Z. Lei, S. Odenbach, and K. Eckert, *Appl. Phys. Lett.* **105**, 232407 (2014).
 - [19] X. Yang, K. Tschulik, M. Uhlemann, S. Odenbach, and K. Eckert, *J. Phys. Chem. Lett.* **3**, 3559 (2012).
 - [20] I. R. Rodrigues, L. Lukina, S. Dehaeck, P. Colinet, K. Binnemans, and J. Fransaer, *J. Phys. Chem. Lett.* **8**, 5301 (2017).
 - [21] Z. Lei, B. Fritzsche, and K. Eckert, *J. Phys. Chem. C* **121**, 24576 (2017).
 - [22] B. Ji, P. Wu, H. Ren, S. Zhang, A. Rehman, and L. Wang, *Chin. Phys. B* **25**, 074704 (2016).
 - [23] K. Kołczyk-Siedlecka, M. Wojnicki, X. Yang, G. Mutschke, and P. Zabinski, *J. Flow Chem.* **9**, 175 (2019).
 - [24] W. Noddack and E. Wicht, *Z. Elektrochem., Ber. Bunsen-Ges. Phys. Chem.* **56**, 893 (1952).

- [25] C. Yan, J. Jia, C. Liao, S. Wu, and G. Xu, *Tsinghua Sci. Tech.* **11**, 241 (2006).
- [26] K. Binnemans, P. T. Jones, B. Blanpain, T. Van Gerven, Y. Yang, A. Walton, and M. Buchert, *J. Clean. Prod.* **51**, 1 (2013).
- [27] W. M. Haynes, *CRC Handbook of Chemistry and Physics* (CRC Press, Boca Raton, FL, 2014).
- [28] J. M. D. Coey, F. Rhen, P. Dunne, and S. McMurry, *J. Solid State Electrochem.* **11**, 711 (2007).
- [29] S. Chandrasekhar, *Hydrodynamic and Hydromagnetic Stability* (Courier Corporation, Mineola, NY, 2013).
- [30] F. Doumenc, T. Boeck, B. Guerrier, and M. Rossi, *J. Fluid Mech.* **648**, 521 (2010).
- [31] M. Heckert, L. Sprenger, A. Lange, and S. Odenbach, *J. Magn. Mater.* **381**, 337 (2015).
- [32] Z. Lei, C. Haberstroh, S. Odenbach, and K. Eckert, *Int. J. Refrig.* **62**, 166 (2016).
- [33] Z. Lei, X. Yang, C. Haberstroh, B. Pulko, S. Odenbach, and K. Eckert, *Int. J. Refrig.* **56**, 246 (2015).
- [34] J. M. D. Coey, *Magnetism and Magnetic Materials* (Cambridge University Press, Cambridge, 2010).